JOURNAL OF APPLIED ELECTROCHEMISTRY 25 (1995) 682–689

Role of minor alloying elements on the performance of lead–acid battery grids Part I: Corrosion of Pb–Se alloys

A. G. GAD ALLAH, H. A. ABD EL-RAHMAN

Department of Chemistry, Faculty of Science, Cairo University, Giza, Egypt

M. ABD EL-GALIL

Chloride, Egypt Company for Batteries, Egypt

Received 18 July 1994; revised 8 December 1994

The corrosion behaviour of Pb–Se alloys (Se: 0.00, 0.01, 0.04 and 0.06%) to be used in the manufacture of grids for pasted lead–acid batteries, was studied under open circuit, potentiostatic and galvanostatic polarization in 5.0 M H_2SO_4 solutions. Selenium was found to shift the corrosion potential to more negative values and increase the sulfation and self-discharge; the extent being dependent on the percentage of selenium. The potentiostatic $E/\log i$ curve was significantly influenced, especially the passivity region from −0.90 to +1.30 V vs Hg/Hg_2SO_4 (1.0 M H_2SO_4), where the passivity current and the critical current and potential to start the nucleation of $PbSO_4$ decreased in the presence of selenium. Both oxygen and hydrogen evolution overpotentials were found to be higher for the alloys containing selenium. In many aspects, the alloy composition Pb–0.04% Se was found to be critical. Factors affecting the constant current charging; the charging time, temperature and the number of charging–discharging cycles, N, were investigated. Generally, the corrodability of Pb–Se alloys was relatively higher and increasing N was found to increase corrosion in the order: Pb–0.04% Se > Pb–0.01% Se > Pb–0.06% Se > Pb. As the charging time increased, the rate of corrosion decreased for Pb–Se alloys while it was constant for Pb.

1. Introduction

The corrosion of the grid of lead–acid batteries plays a key role in determining the durability and the life of the battery. Numerous lead alloys have been tested for the manufacture of grids of pasted batteries, especially Pb–Sb and Pb–Ca without or with other elements [1–28]. Although many lead alloys have desirable mechanical and casting properties, they suffer more or less from electrochemical corrosion, mostly due to overcharging and self-discharging. In severe cases of corrosion the battery fails to supply the expected energy and/or can not be recharged effectively. The widely used Pb–Sb grids usually contain minute amounts of other elements either purposely or as impurities and these elements have a noticeable influence on the grid performance [1, 6, 9, 13–15, 27].

To explore the effect of minor alloying elements (namely, Se, As, Sn and Cu) on the corrosion behaviour of Pb–Sb grids, it is intended to study the corrodability of binary alloys of Pb and each of Se, Sn, As and Cu, separately at first. Subsequently, some combined Pb–Sb–Se–As–Sn–Cu alloys will be investigated. These low antimony alloys have recently received some interest [22, 24, 29–31] and are currently used in the manufacture of grids at the Chloride Egypt Company for Batteries.

This paper reports work on the behaviour of Pb–Se alloys (Se%: 0.00, 0.01, 0.04 and 0.06) under open-circuit and potentiostatic and galvanostatic polarization in 5.0 M H_2SO_4 solutions under different conditions.

2. Experimental details

The electrodes in the form of discs (apparent surface areas 0.196 cm^2) were cut from cylindrical rods of spectroscopically pure lead (Johnson–Matthey) and Pb–Se alloys (nominal Se%: 0.01, 0.04 and 0.06). The alloys were cast by addition of known weights of specpure Se under nitrogen atmosphere to molten lead at 500 °C. The temperature was maintained for three hours to ensure complete dissolution of selenium, then the melt was poured in cylindrical ceramic moulds and the cast rods were removed from the moulds at about 150 °C. The exact percentages of selenium in the alloys were determined by atomic absorption spectrophotometer (Perkin–Elmer 2380) to be 0.011, 0.039 and 0.062 for Pb–0.01% Se, Pb–0.04% Se and Pb–0.06% Se, respectively. The electrodes were mechanically polished with successively finer grades of emery paper down to 4/0, 0.05 μm alumina, cleaned thoroughly on wet tissue and, finally, rinsed with distilled water. 5.0 M H_2SO_4 solutions were

0021-891X

prepared from AR grade sulphuric acid stock and triply distilled water. All potentials were measured and referred to a $Hg/Hg_2SO_4/1.0\,M H_2SO_4$ reference electrode. The electrolytic cell and the Wien type a.c. bridge were essentially the same as described elsewhere [32]. The cell impedance was balanced against a series connection of calibrated variable resistance and capacitance boxes at 1.0 kHz. After attainment of the steady state, the effect of frequency, f, on C and R was traced in the range 200–10 000 Hz. Complex plane impedance plots $(2\pi fC)^{-1}$ against R were drawn and the phase shift angle, $\theta = d(2\pi fC)^{-1}/dR$, was determined. Steady potentiostatic polarization curves were traced with the aid of a scanning potentiostat (EG&G Model 362) and a digital multimeter. Galvanostatic polarization was carried out by using an electronic constant current unit and an X–Y recorder (Cole–Parmer model LY 1400). All experiments were carried out at constant temperature of 30 ± 0.1 °C in a double walled electrically controlled air thermostat.

3. Results and discussion

3.1. *Open-circuit sulphation*

The open-circuit potential, E_{oc}, the capacitance, C, and the resistance, R, of the electrodes were traced with time in 5.0 M H_2SO_4 solution at 30 °C until more or less stable values were attained. As seen in

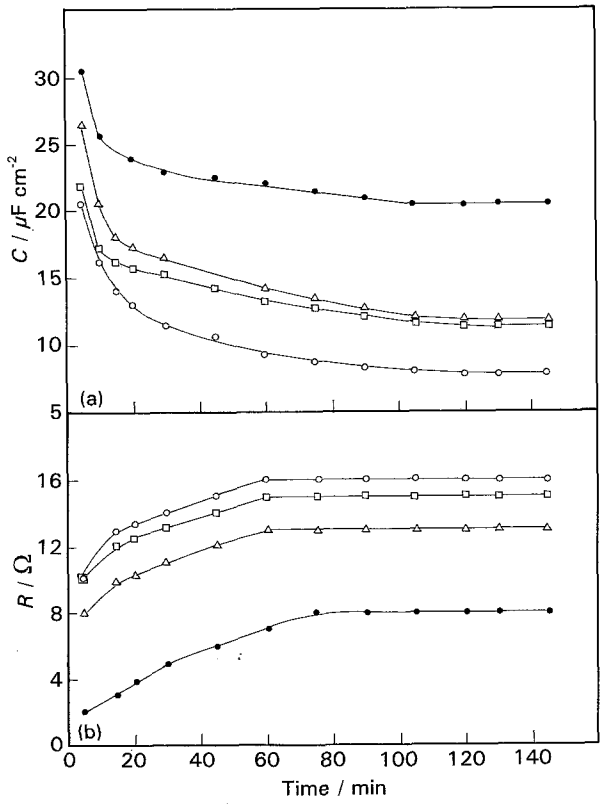

Fig. 1. Variation of capacitance, C, (a) and resistance, R, (b) of Pb–Se electrodes in 5.0 M H_2SO_4 solutions at 30 °C: (●) Pb, (△) Pb–0.01% Se, (□) Pb–0.04 Se and (○) Pb–0.06% Se. Frequency: 1.0 kHz.

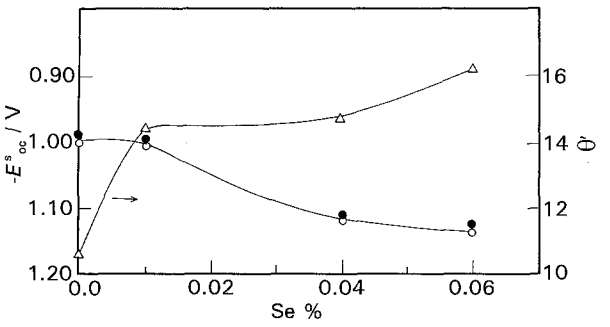

Fig. 2. Dependence of the steady open circuit potential, E^s_{oc} (○) and the parameter θ' (△) on Se%. The horizontal arrow refers to the redox potential $Pb/PbSO_4$ in 5.0 M H_2SO_4, (●) E_{oc} at zero time.

Fig. 1, C decreases and R increases with time as a result of sulphate layer formation. At the steady state, the faradaic contribution is negligible and the capacitance is approximately given by:

$$C/\sigma = C_{dl}(1-\theta) + \theta C_s \qquad (1)$$

where C_{dl} is the double layer capacitance in the absence of specific adsorption, C_s is the sulphate layer capacitance, θ is the surface coverage and σ is the roughness factor. Equation 1 may be used to estimate the degree of surface coverage by monolayer adsorbed organic inhibitors [33, 34]. The roughness factor was estimated by extrapolation of C to zero time, i.e. $\theta \rightarrow 0$, and thus

$$\sigma = \frac{C_{t\rightarrow o}}{C_{dl}} \qquad (2)$$

From the literature, $C_{dl} \simeq 17\,\mu F\,cm^{-2}$ [35] and the average σ was found to be 2.5. For the sake of comparison, the parameter $\theta' = \theta(C_{dl} - C_s) = C_{dl} - C/\sigma$ was calculated to represent the degree of surface sulphation. Fig. 2 shows the dependence of θ' and the steady open-circuit potential, E^s_{oc}, on Se%. As the percentage of Se increases, θ' increases and E^s_{oc} shifts to more negative values. This indicates that the corrodability of the alloy and formation of sulphate increases with percentage of Se. It seems that selenium activates the sulfation process by acting as a cathodic centre for oxygen reduction or hydrogen evolution. Table 1 summarizes the most probable redox processes for Pb in H_2SO_4 at 30 °C. The observed E^s_{oc} values are close to the reversible potential of $PbSO_4$ formation. Figure 3 shows the complex plane impedance plots for the alloys in 5.0 M H_2SO_4 solutions (frequency range 200–10 000 Hz). The capacitative component (imaginary part) of the impedance varies linearly with the resistive component (real part) and the impedance tends to be capacitative as the percentage of Se increases. The deviation of the phase shift angle, θ, from the purely capacitative value ($\theta = 90°$) indicates that the sulphate layer can not be treated as a perfect dielectric and leakage through the layer occurs. As the percentage of Se increases the insulating properties of the layer increase in agreement with the reported increase of the surface coverage θ' (Fig. 2).

Table 1. Redox processes of lead in H_2SO_4 acid solutions, standard redox potential, $E°$, and the redox potential in 5.0 M H_2SO_4 solutions at 30 °C, E

Process	$E°$/V (*vs* $Hg/Hg_2SO_4/1.0$ M H_2SO_4)	E/V
$PbSO_4 + 2e^- = Pb + SO_4^{2-}$ $E = E° - 0.03 \log a_{SO_4^{2-}}$	−1.038	−1.044
$PbO + 2H + 2e^- = Pb + H_2O$ $E = E° - (0.06/2) \log a^2_{H^+}/a_{H_2O}$	−0.434	−0.452
$PbO \cdot PbSO_4 + 2H^+ + 4e^- = 2Pb + SO_4^{2-} + H_2O$ $E = E° - (0.06/4) \log a^2_{H^+}/a_{SO_4^{2-}} \times a_{H_2O}$	−0.795	−0.801
$3PbO \cdot PbSO_4 \cdot H_2O + 6H^+ + 8e^- = 4Pb + SO_4^{2-} + 4H_2O$ $E = E° - (0.06/8) \log a^6_{H^+}/a_{SO_4^{2-}} \times a^4_{H_2O}$	−0.652	−0.660
$PbO_2 + 2H^+ + 2e^- = PbO + H_2O$ $E = E° + (0.06/2) \log a^2_{H^+}/a_{H_2O}$	0.425	0.443
$PbO_2 + 4H^+ + SO_4^{2-} + 2e^- = PbSO_4 + 2H_2O$ $E = E° - (0.06/2) \log a^4_{H^+} a_{SO_4^{2-}}/a^2_{H_2O}$	1.005	0.962

For 5.0 M H_2SO_4, the mean activity coefficient, $\gamma\pm = 0.25$ and molality, $m = 6.3$. Total activity of H_2SO_4, $a = 4\gamma^3$. The activity of water in 5.0 M H_2SO_4 solution was taken 0.6 [35].

3.2. *Potentiostatic polarization*

Prior to polarization, the electrodes were held at a potential of −1.6 V for 30 min to remove any surface reducible layers. The potential was then increased in the anodic direction in 10–50 mV steps and the respective quasisteady current was recorded within 2–10 min. The potential was changed from −1.600 to +1.800 V to cover the range of the hydrogen evolution to oxygen evolution region. Anodic $E/\log i$ curves for Pb–Se alloys in 5.0 M H_2SO_4 solutions are shown in Fig. 4, where a significant effect of selenium is observed, especially, in the passive region from −0.900 to 1.300 V. In region I (−1.0 V to E_c), the current increases due to the almost reversible dissolution of Pb to Pb^{2+} [36] until a critical passivation potential, E_c, is attained, where $PbSO_4$ starts to precipitate. Thereafter the current decreases rapidly to a more or less short passive region II′ ($i \simeq 0.03$ mA cm^{-2}) before it decreases again and passivity is established. The length of region II′ decreases as the percentage of Se increases; this behaviour is related to the formation of the primary passivating $PbSO_4$ layer. The passivity current, i_p^{II}, was taken as the minimum current recorded in region II ($PbSO_4$ formation region). It should be mentioned that i_p^{II} for lead is

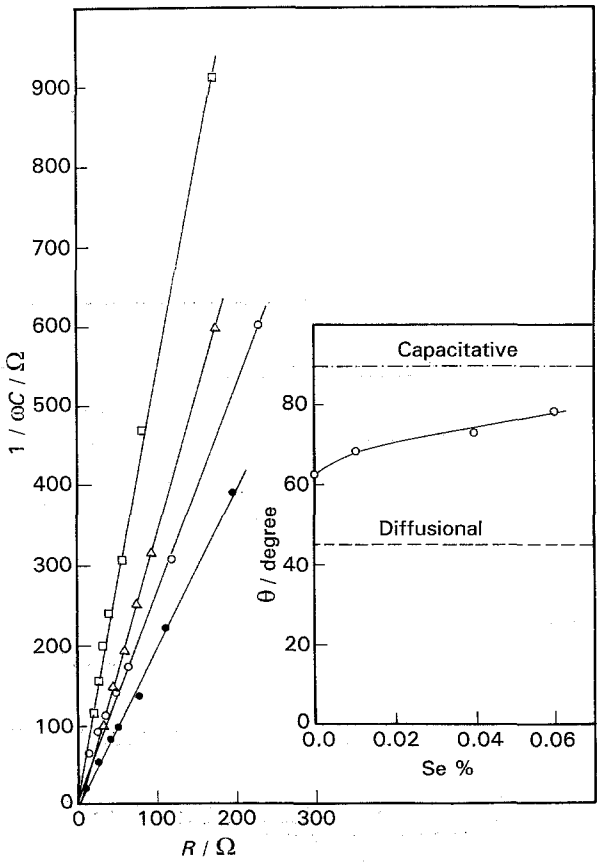

Fig. 3. Complex plane impedance plots for Pb–Se alloys in 5.0 M H_2SO_4 solutions at 30 °C after the attainment of the steady state. (●) Pb, (○) Pb–0.01% Se, (△) Pb–0.04% Se and (□) Pb–0.06% Se. Inset: Phase shift, θ, against Se%. (– · – · –) Pure capacitative impedance and (– – – –) diffusional 'Warburg' impedance.

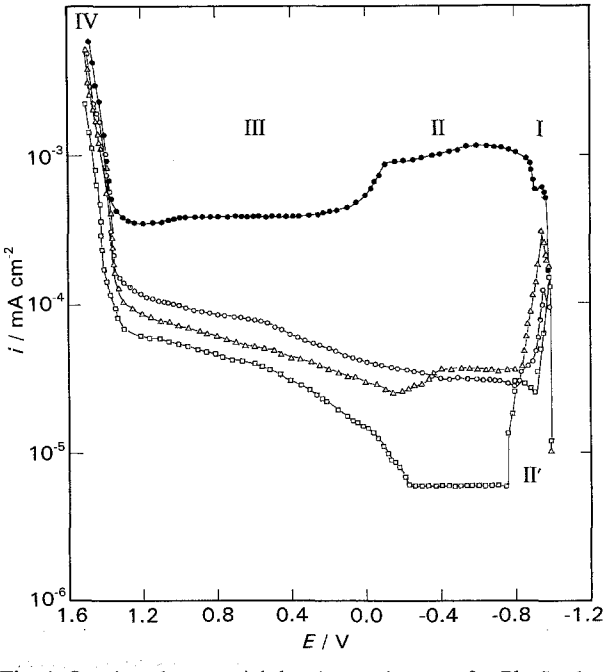

Fig. 4. Quasisteady potential–log (current) curves for Pb–Se electrodes in 5.0 M H_2SO_4 solutions at 30 °C: (●) Pb, (△) Pb–0.01% Se, (□) Pb–0.04% Se and (○) Pb–0.06% Se.

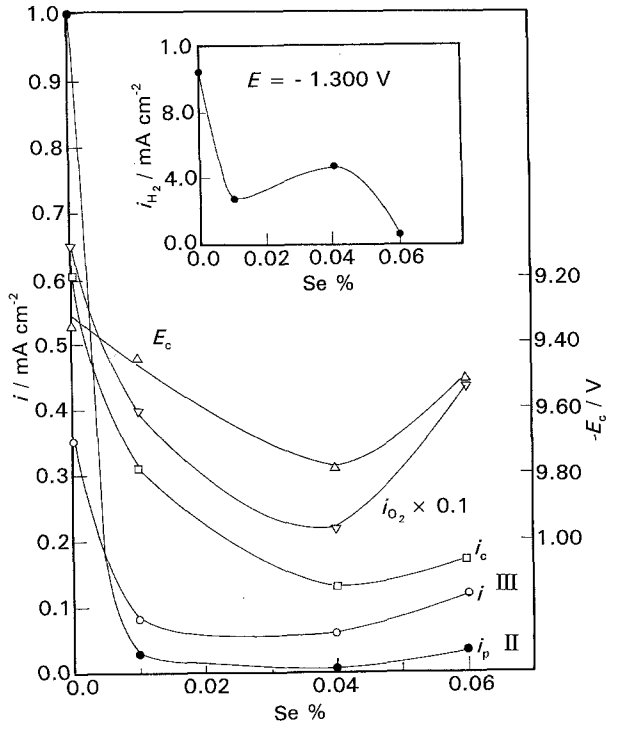

Fig. 5. Dependence of the critical passivation potential, E_c (△) and current, i_c (□), the passivity current, i_P^{II} (●), the current in region III at $E = 1.200$ V, i^{III} (○) and the oxygen evolution current at $E = 1.500$ V, i_o (▽) on Se%. Inset: hydrogen evolution current at $E = -1.300$ V, i_{H_2} against Se%.

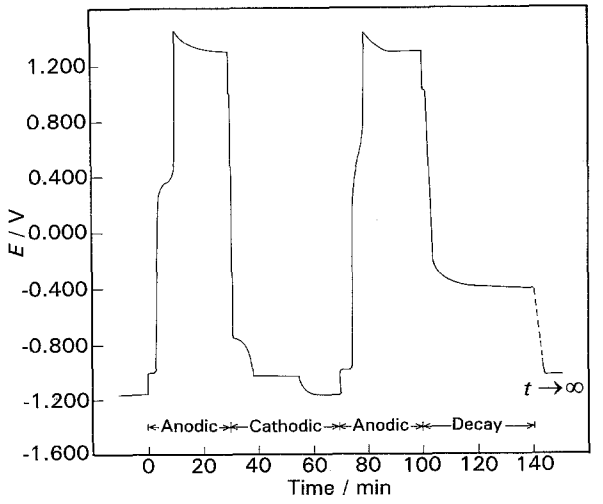

Fig. 6. Alternative anodic–cathodic–anodic polarization at 255 μA cm^{-2} and the following potential decay for Pb–0.04% Se in 5.0 M H_2SO_4 solutions at 30 °C.

even higher than the critical passivation current, i_c, in contrast to Pb–Se alloys.

In region III, PbO grows under the $PbSO_4$ layer [17, 37–39] and the current, i^{III}, increases gradually until the onset of oxygen evolution. The current in region III for lead is practically constant but still much higher than for Pb–Se alloys. Oxygen evolution and PbO_2 formation occur in region IV. Selenium appears to inhibit oxygen evolution but without a noticeable effect on the reaction mechanism. A similar effect was observed on the hydrogen evolution reaction.

Figure 5 shows the dependence of the various electrochemical parameters on the percentage of Se. All the parameters, E_c, i_c, i_p^{II}, i^{III} and i_{O_2}, i_{H_2}, decrease in the presence of selenium and the alloy Pb–0.04% Se seems to be a critical composition. Among the Pb–Se alloys tested, Pb–0.04% Se showed the best passivity, the highest oxygen overpotential and the lowest hydrogen overpotential.

3.3. *Galvanostatic polarization*

The electrodes were subject to the following galvanostatic polarization program at 255 μA cm^{-2} (in sequence): cathodic polarization until the potential became steady → charging for 30 min → discharging to the steady potential before charging → a second charging for 30 min → circuit opening and reading of potential decay. Figure 6 illustrates the galvanostatic polarization curve for Pb–0.04% Se in 5.0 M H_2SO_4 solution and the different electrochemical processes at the observed potential arrests are summarized in Table 2. The arrests corresponding to $PbSO_4$ formation and $PbSO_4$ and PbO · $PbSO_4$ reduction occur very close to the respective redox potentials (cf. Tables 1 and 2). The arrest at ~ 0.40 V is much less pronounced for Pb–0.01% Se and Pb–0.06% Se. It occurs close to the reversible potential of PbO/PbO_2 transformation and refers to the start of PbO_2 formation from lower oxides under the sulphate layer. The highly protective $PbSO_4$ layer impedes the transport of sulphate species to the metal surface and the environment under the layer becomes less acidic, that is, PbO formation is more favoured. Potentiostatic results revealed that the highest passivity ($PbSO_4$ layer protection) is due to Pb–0.04% Se which agrees with the more pronounced appearance of the arrest at about 0.40 V. The quasisteady potential reached after current interruption is very close to the PbO/Pb redox potential ~ −0.40 V and indicates the transformation of PbO_2 → PbO during the decay. After much longer times (depending on the charging capacity), E_{oc}^{s} is reached due to the transformation of PbO to the thermodynamically more stable $PbSO_4$ in 5.0 M H_2SO_4 solutions. During the potential decay, substantial variations in C and R occurred as can be seen in Fig. 7. The decrease in C and increase in R with time indicate the growth of an insulating layer. This is consistent with the transformation of the conducting PbO_2 into the insulating PbO and $PbSO_4$ by a self-discharge process. The potential decay of a thin PbO_2 layer ($Q = 1.8$ C cm^{-2}) showed a linear variation with time at the beginning of the self-discharge process (excluding the first 1–3 min). The initial rate of potential decay increased significantly in the presence of selenium (cf. Fig. 7). This confirms the role of selenium in enhancing the self-discharging. In this respect, Pb–0.04% Se shows the least effect. It should be noted that no arrest was observed for PbO_2 → PbO transformation during discharge but a very short arrest corresponding to PbO_2 → $PbSO_4$ occurred at ~ 1.0 V. The arrest period of the latter process was found to be much smaller than those of $PbSO_4$ and

Table 2. Electrochemical processes occurring during the cyclic galvanostatic polarization at c.d. = 255 $\mu A\,cm^{-2}$ for Pb–Se alloys in 5.0 M H_2SO_4 solutions at 30 °C

Process	*%Se*	*E*/V	Q^*/C cm^{-2}	$I^f_{PbO_2}$
First oxidation arrest (sulphate formation)	0.00	−0.980	0.031	
	0.01	−0.998	0.107	
	0.04	−1.000		
	0.06	−1.000		
Second oxidation arrest	0.00	‡	‡	
	0.01	‡	‡	
	0.04	0.36		
	0.06	†	†	
Third oxidation arrest (oxygen evolution and oxide formation)	0.00	1.40	0.413	0.72
	0.01	1.28	0.337	0.99
	0.04	1.30	0.413	0.83
	0.06	1.30	0.352	0.83
First reduction arrest ($Pb^{4+} \rightarrow Pb^{2+}$)	0.00	1.14	0.038	
	0.01	1.10	†	
	0.04	1.04	0.015	
	0.06	1.07	†	
Second reduction arrest (basic sulphate reduction)	0.00	−0.74	0.115	
	0.01	−0.80	0.092	
	0.04	−0.78	0.107	
	0.06	−0.78	0.061	
Third reduction arrest (sulphate reduction)	0.00	−1.04	0.214	
	0.01	−1.04	0.362	
	0.04	−1.04	0.275	
	0.06	−1.03	0.321	
Quasisteady decay potential after charging	0.00	−0.36		
	0.01	−0.44		
	0.04	−0.40		
	0.06	−0.41		

* Q value are given for the 1st cycle.
† Arrest does not appear well defined.
‡ Arrest is absent.

$PbO \cdot PbSO_4$ reduction. This is attributed to the self-discharge process between the PbO_2 layer and the underlying lead (Pb) which runs parallel to the electrochemical reduction of PbO_2. As a result, the amount of Pb^{2+} species increases substantially. The self-discharge of PbO_2 also occurs through oxygen evolution and hydrogen oxidation [6, 40, 41].

The charge densities, Q, consumed in the various electrochemical processes (arrest time × current density) are given in Table 2. The total anodic and cathodic charge densities, Q_{ca} and Q_{an}, are given by

$$Q_{an} = Q^f_{PbSO_4} + Q^f_{PbO_2} + Q^f_{O_2} \quad (3)$$

$$Q_{ca} = Q^r_{PbO_2} + Q^r_{PbO \cdot PbSO_4} + Q^r_{PbSO_4} \quad (4)$$

where superscripts 'f' and 'r' refer to formation and reduction, respectively, and the charges consumed in soluble Pb^{2+} formation and oxygen reduction are neglected. It is also assumed that self-discharge occurs essentially according to the reaction [41]

$$PbO_2 + Pb + 2H_2SO_4 = 2PbSO_4 + 2H_2O \quad (5)$$

The charge due to the self discharging (Equation 5), Q_{SD}, is given by

$$Q_{SD} = 1/2(Q^r_{PbO \cdot PbSO_4} + Q^r_{PbSO_4}) - Q^r_{PbO_2} \quad (6)$$

and the charge consumed in PbO_2 formation, $Q^f_{PbO_2}$, is thus

$$Q^f_{PbO_2} = 2(Q^r_{PbO_2} + Q_{SD}) \quad (7)$$

The efficiency of PbO_2 formation, I^f_{PbO}, can be estimated from the relation:

$$I^f_{PbO_2} = \frac{(Q^r_{PbO \cdot PbSO_4} + Q^r_{PbSO_4})}{Q_{an}} \quad (8)$$

As may be seen in Table 2, the efficiency of PbO_2 formation increases in the presence of selenium and, consequently, oxygen evolution should decrease as observed in the potentiostatic part. Table 2 shows that Q_{ca} is essentially the charge consumed in the reduction of Pb^{2+} which results mainly from the self-discharge of PbO_2.

Q_{ca} may be taken as an index for the corrodability of the alloy under one and the same conditions. In the following part, the factors affecting the corrodability are presented.

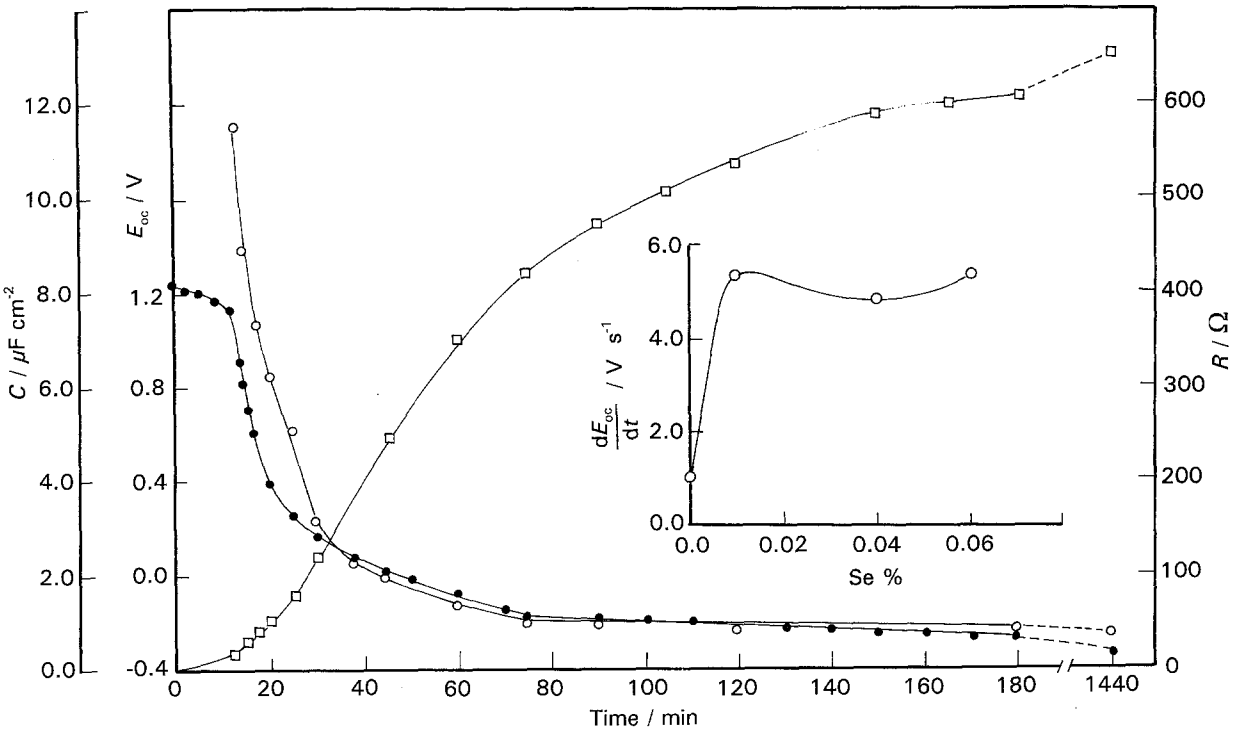

Fig. 7. Variation of the open circuit potential, E_{oc}, capacitance, C, and resistance, R, of Pb–0.04% Se electrode with time after interrupting the charging current. The current 510 μA cm^{-2} was passed for 3 h. The solution was 5.0 M H_2SO_4. Temperature: 30 °C. Inset: initial rate of potential decay, dE_{oc}/dt against Se%. The alloys were charged at 510 μA cm^{-2} for 60 min before the decay.

3.3.1. Charging time. The electrodes were charged with a constant current density of 255 μA cm^{-2} for different times and the respective Q_{ca} values were determined from the discharge E/time curves. Figure 8 shows that Q_{ca} increases linearly with the charging time for lead whereas Q_{ca} decreases with the charging time for Pb–Se alloys. Up to 90 min charging, Q_{ca} for Pb–Se alloys is higher than that of Pb but the situation is reversed at longer charging times, i.e. Q_{ca} for Pb is higher. The results may be explained in terms of change in efficiency of PbO_2 formation during the charging process. Potentiostatic and galvanostatic results showed that the efficiency of PbO_2 formation is relatively higher for Pb–Se due to the increase in overpotential of the oxygen evolution reaction. This situation seems to be fulfilled in the early stages of PbO_2 formation. As the charging becomes deeper, the probability of oxygen evolution on the formed PbO_2 layer rather than on the underlying metal surface increases. It appears that the kinetics of oxygen evolution on the PbO_2 layer formed on Pb–Se alloys are more facile than on those on Pb. This may be due to the physical and chemical properties of the growing PbO_2 layer and the initially formed $PbSO_4$ layer. The important conclusion is that grids made of Pb–Se alloys suffer relatively less corrosion when subject to prolonged charging; Pb–0.01% Se < Pb–0.04% Se < Pb–0.06% Se < Pb.

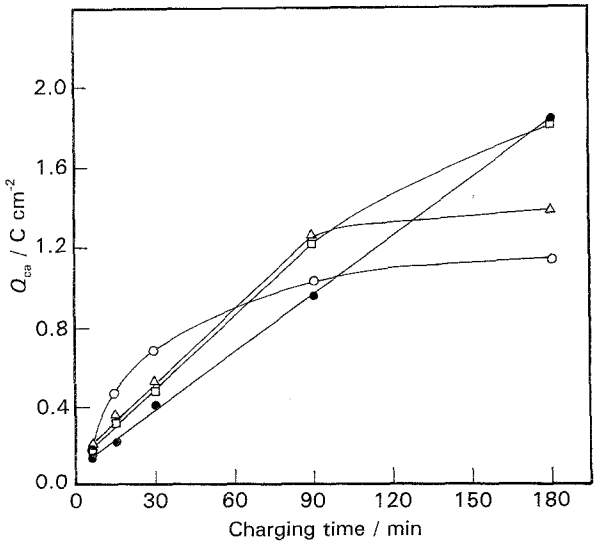

Fig. 8. Total cathodic charge, Q_{ca} against the charging time. The electrodes were charged and discharged at 255 μA cm^{-2} in 5.0 M H_2SO_4 solutions. Temperature: 30 °C, (●) Pb, (○) Pb–0.01% Se, (△) Pb–0.04% Se and (□) Pb–0.06% Se.

3.3.2. Charging rate and temperature. The Pb–0.04% Se alloy was charged by using different current densities until a constant charge was consumed (Q_{an} = 5.08 C cm^{-2}) and the respective Q_{ca} values were determined from the discharge curves at 255 μA cm^{-2} and 30 °C. At different temperatures, the alloy was also charged for 60 min at 255 μA cm^{-2} and discharged at the same current density (c.d.). As can be seen in Fig. 9, Q_{ca} decreases markedly as c.d. increases while it increases as temperature rises up to 30 °C, then decreases slowly. The decrease in PbO_2 formation efficiency as c.d. increases may be attributed to the decrease in oxygen evolution overpotential. Thus, charging at higher current densities is associated with lower corrodability of the grid. The increase in PbO_2 formation efficiency as temperature rises is usually explained in

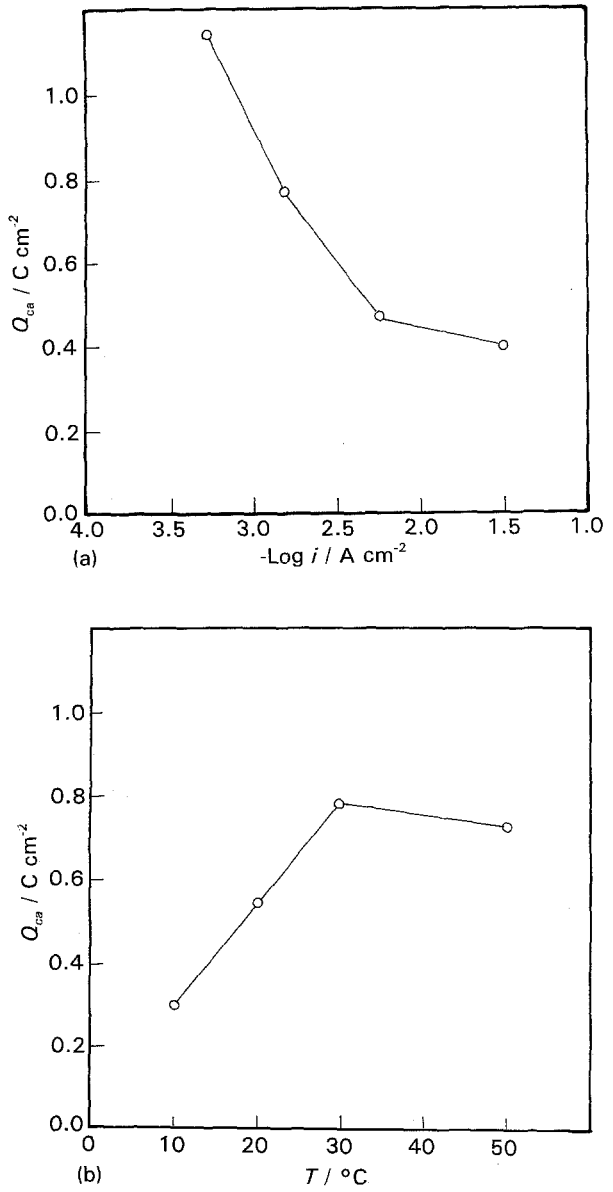

Fig. 9. Dependence of the total cathodic charge, Q_{ca}, on logarithm of current density (a) and temperature (b). Details in text.

terms of improving the electrolyte performance (resistivity and viscosity) [42]. At temperatures $>30\,°C$, the electrolyte has a negligible effect and the efficiency starts to decrease with rising temperature probably due to the increase in charge consumed in the formation of the $PbSO_4$ layer, the solubility of which increases with rising temperature [43].

3.3.3. Charging cycles. The alloys were subjected to alternative cathodic and anodic polarization cycles at c.d. $5.1\,mA\,cm^{-2}$ in $5.0\,M$ H_2SO_4 solutions (half cycle time: 10 min) and Q_{ca} was determined by discharge at $255\,\mu A\,cm^{-2}$. The time of the cathodic half cycle was found to be sufficient to ensure complete discharge. After complete discharge, the polarity was reversed and the charge consumed in $PbSO_4$ formation, $Q^f_{PbSO_4}$, was determined. Figure 10 shows the dependence of Q_{ca} on the number of polarization cycles, N. Q_{ca} increases linearly with N for Pb–0.01% Se, irregularly but substantially for Pb–0.04% Se and almost negligibly for Pb–0.06% Se and Pb. After a few cycles, Q_{ca} is generally higher for Pb–Se alloys and Pb–0.04% Se shows the greatest effect of cycling on the efficiency of PbO_2 formation. Due to the self-discharge process, the polarization cycles are expected to increase the corrodable layer thickness, that is, thicker spongy-sulphate layer growth. $Q^f_{PbSO_4}$ is a measure of the thickness of such a layer and is shown as a function of number of polarization cycles in Fig. 11. The figure shows clearly that the corrodable layer thickness increases with increasing number of polarization cycles and Se content. It is concluded that the corrodability of the grid made of Pb–Se alloys increases substantially as the number of charging–discharging cycles increases.

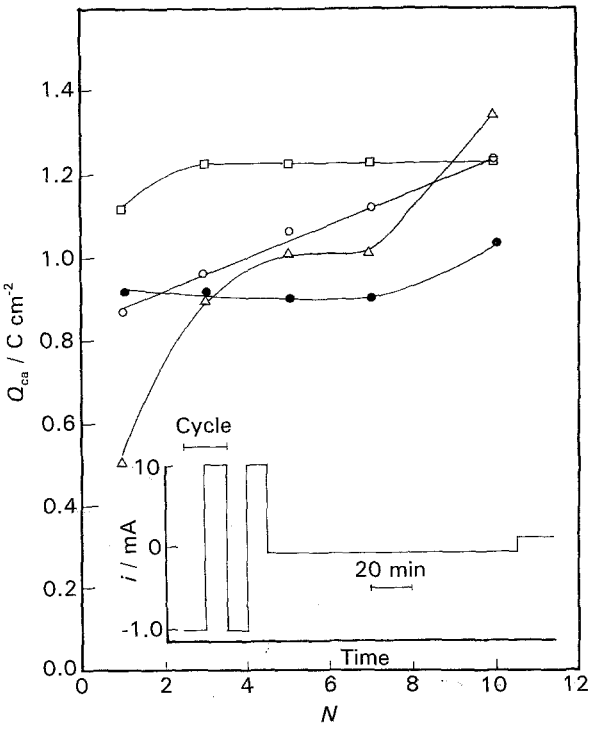

Fig. 10. Dependence of the total cathodic charge, Q_{ca}, on the number of galvanostatic polarization cycles, N. Lower part of the Figure shows the polarization program. Temperature: 30° C. Electrolyte: $5.0\,M$ H_2SO_4. (●) Pb, (○) Pb–0.01% Se, (△) Pb–0.04% Se and (□) Pb–0.06% Se.

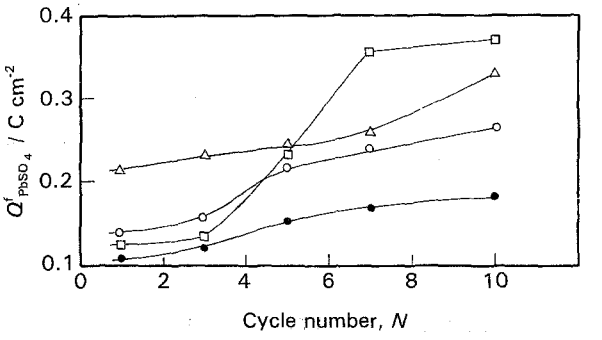

Fig. 11. Dependence of the charge consumed in $PbSO_4$ formation, $Q^f_{PbSO_4}$ on the number of polarization cycles, N. Temperature: 30 °C. Electrolyte: $5.0\,M$ H_2SO_4. (●) Pb, (○) Pb–0.01% Se, (△) Pb–0.04% Se and (□) Pb–0.06% Se.

4. Conclusion

Selenium was found to affect the electrochemical

behaviour of lead in 5.0 M H_2SO_4 solutions. It increases the sulphation and enhances the discharge process. Corrosion during charging also increases due to the increase in the oxygen evolution overpotential. The alloy Pb–0.04% Se was found to be critical among the different Pb–Se alloys; passivity current, self-discharge rate, hydrogen evolution overpotential and critical passivation potential are minimum for this composition.

References

[1] N. A. Novikova, V. P. Derevyagina, I. S. Dankova, N. V. Milovidova, M. A. Dasoyan and A. A. Ravdel, *Zh. Prikl. Khim.* **44** (1971) 2447.
[2] A. A. Abdul Azim and K. M. El-Sobki, *Corros. Sci.* **12** (1972) 371.
[3] H. Bode, 'Lead-acid batteries', John Wiley & Sons, New York (1977), p. 238.
[4] G. Kawamura, S. Mochizuki and A. Komaki, *Denki Kagaku Oyobi Kogyo Butsuri Kagaku* **48** (1980) 554.
[5] A. Komaki, G. Kawamura and S. Mochizuki, *Prog. Batteries Sol. Cell* **4** (1982) 167.
[6] V. Iliev and D. Pavlov, *J. Electrochem. Soc.* **129** (1982) 458.
[7] J. A. Bialacki, N. A. Hampson and K. Peters, *ibid.* **130** (1983) 1797.
[8] S. Sternberg, V. Bronzoi, L. Apateau and A. Mateescu, *Rev. Roum. Chim.* **28** (1983) 83.
[9] W. Zhon and X. Chen, *Huoxue Xuebao* **43** (1985) 333; *ibid.* **44** (1986) 399.
[10] M. Maja and P. Spinelli, *Werkst. Korros.* **36** (1985) 554.
[11] F. Molnar and S. Spakovska, *Pokroky Praskove Metal.* **4** (1985) 48.
[12] B. K. Mahata, J. L. Strebe, D. F. Wilkinson and K. R. Bullock, *J. Electrochem. Soc.* **132** (1985) 19.
[13] A. G. Mateescu and D. C. Mateescu, *Rev. Chem. (Bucharest)* **37** (1986) 906.
[14] S. Webster, P. J. Mitchell, N. A. Hampson and J. I. Dyson, *J. Electrochem. Soc.* **133** (1986) 133.
[15] S. Webster, P. J. Mitchell and N. A. Hampson, *ibid.* **133** (1986) 137.
[16] A. H. Le, Proceedings of the International Power Sources Symposium, 32nd (1986) 351.
[17] M. N. C. Ijomah, *J. Electrochem. Soc.* **134** (1987) 2960.
[18] T. Take and K. Akuto, *Rev. Electr. Commun. Lab.* **36** (1988) 481.
[19] A. G. Mateescu and D. C. Mateescu, *Rev. Roum. Chim.* **33** (1988) 595.
[20] T. Rogachev, *J. Power Sources* **23** (1988) 331.
[21] R. Janakiraman, P. G. Balakrishnan, M. Devasahayam and S. Palanichamy, *Bull. Electrochem., India* **4** (1988) 563.
[22] H. Yoshinga, T. Ozaki and S. Fukuda, *Kokai Tokkyo Kohi JP 02 262 257* (1990).
[23] D. Pavalov and K. Kapkov, *J. Electrochem. Soc.* **137** (1990) 16.
[24] H. Lin, P. Xu and W. Zhou, *Yengyong Huxue* **8** (1991) 60.
[25] D. Pavalov, A. Dakhouche and T. Rogachev, *J. Power Sources* **42** (1993) 71.
[26] P. Peat, P. T. Moseley, A. F. Hollenkamp and D. A. Rand, *ibid.* **42** (1993) 119.
[27] J. Sklarchuk, M. J. Dewan, E. M. Valeriote and A. M. Vincze, *ibid.* **42** (1993) 47.
[28] Z. W. Chen, J. B. See, W. F. Gillian and D. M. Rice, *ibid.* **42** (1993) 35.
[29] J. Cerny, F. Kalab, J. Miskovsky, M. Matejka, Karel, *Czech. C.S.* **262** (1990) 883.
[30] S. Osumi and T. Omae, *Jpn. Kokai Tokkyo Koho JP 04 02 055* (1990).
[31] Y. Huang, *Faming Zhuanli Shenging Gongkai Shuoming Shu CN 1 055 204*(1991).
[32] A. G. Gad-Allah, H. A. Abd El-Rahman, S. A. Salih and M. Abd El-Galil, *J. Appl. Electrochem.* **22** (1992) 571.
[33] A. G. Gad-Allah, W. A. Badawy, H. H. Rehan and M. M. Abou-Romia, *ibid.* **19** (1989) 928.
[34] H. A. Abd El-Rahman, *Corrosion* **47** (1991) 424.
[35] H. S. Harned and W. J. Hamer, *J. Am. Chem. Soc.* **57** (1935) 27.
[36] L. M. Baugh, K. L. Bladen and F. L. Tye, *J. Electroanal. Chem.* **145** (1983) 355.
[37] K. R. Bullock, G. M. Trischan and R. G. Burrow, *J. Electrochem. Soc.* **130** (1983) 1283.
[38] K. R. Bullock and M. A. Butler, *ibid.* **133** (1986) 1085.
[39] Y. Yamamoto, F. Koichi, T. Veda and M. Nambu, *Electrochim. Acta* **37** (1992) 199.
[40] K. R. Bullock and E. C. Laird, *J. Electrochem. Soc.* **129** (1982) 1393.
[41] J. S. Symanski, B. K. Mahato and K. R. Bullock, *ibid.* **135** (1988) 548.
[42] G. W. Vinal, 'Storage batteries', p. 218, 4th Edn., John Wiley & Sons, New York (1962).
[43] W. J. Hamer, *J. Am. Chem. Soc.* **57** (1935) 9.